crystals

MDPI

Article

Theoretical Study of the Magnetic Properties of the $SmFe_{12-x}Mo_x$ (x = 1, 2) and $SmFe_{10}Mo_2H$ Compounds

Diana Benea [1,*], Eduard Barna [1], Viorel Pop [1] and Olivier Isnard [2]

[1] Faculty of Physics, Babeş-Bolyai University Cluj-Napoca, Kogălniceanu Str. 1, 400084 Cluj-Napoca, Romania; eduard.barna@stud.ubbcluj.ro (E.B.); viorel.pop@ubbcluj.ro (V.P.)
[2] Université Grenoble Alpes, Institut Néel, CNRS, BP166X, CEDEX 9, F-38042 Grenoble, France; olivier.isnard@neel.cnrs.fr
* Correspondence: diana.benea@ubbcluj.ro

Abstract: We present theoretical investigations examining the electronic and magnetic properties of the $SmFe_{12-x}Mo_x$ (x = 1, 2) and $SmFe_{10}Mo_2H$ compounds, including magneto-crystalline anisotropy, magnetic moments, exchange-coupling parameters, and Curie temperatures. The spin-polarized fully relativistic Korringa–Kohn–Rostoker (SPR-KKR) band structure method has been employed, using the coherent potential approximation (CPA) to deal with substitutional disorder. Hubbard-U correction was applied to the local spin density approximation (LSDA+U) in order to account for the significant correlation effects arising from the *4f* electronic states of Sm. According to our calculations, the total magnetic moments increases with H addition, in agreement with experimental data. Adding one H atom in the near-neighbor environment of the Fe *8j* site reduces the magnetic moments of Fe *8j* and enhances the magnetic moment of Fe *8f*. For every investigated alloy, the site-resolved spin magnetic moments of Fe on the *8i*, *8j*, and *8f* sites exhibit the same magnitude sequence, with m_s^{Fe} (*8i*) > m_s^{Fe} (*8j*) > m_s^{Fe} (*8f*). While the addition of H has a positive impact on magneto-crystalline anisotropy energy (MAE), the increase in Mo concentration is detrimental to MAE. The computed exchange-coupling parameters reveal the highest values between the closest Fe *8i* spins, followed by Fe *8i* and Fe *8j* spins, for all investigated alloys. The Curie temperature of the alloys under investigation is increased by decreasing the Mo concentration or by H addition, which is qualitatively consistent with experimental findings.

Keywords: ab initio calculations; magneto-crystalline anisotropy; Curie temperature; permanent magnets

check for updates

Citation: Benea, D.; Barna, E.; Pop, V.; Isnard, O. Theoretical Study of the Magnetic Properties of the $SmFe_{12-x}Mo_x$ (x = 1, 2) and $SmFe_{10}Mo_2H$ Compounds. *Crystals* **2024**, *14*, 598. https://doi.org/10.3390/cryst14070598

Academic Editor: Antonio Frontera

Received: 8 June 2024
Revised: 21 June 2024
Accepted: 25 June 2024
Published: 27 June 2024

Copyright: © 2024 by the authors. Licensee MDPI, Basel, Switzerland. This article is an open access article distributed under the terms and conditions of the Creative Commons Attribution (CC BY) license (https://creativecommons.org/licenses/by/4.0/).

1. Introduction

Many devices utilize magnetic materials as their primary component, and increasing energy efficiency across a wide range of industries depends on the development, impact, and innovation of these materials. Permanent magnets are frequently employed in modern technologies such as magnetic levitation, electric vehicles, windmills, memory devices, transportation, and biomedical devices (e.g., pacemakers, heart pumps, and magnetic resonance imaging machines). As a key part of electric motors, permanent magnets contribute to lower carbon dioxide emissions and lower electricity consumption. The permanent magnets demand is high in green technologies, which use considerable amounts of such materials. Although a permanent magnet must meet a number of properties, its magneto-crystalline anisotropy (MCA), coercivity, and magnetization are the key indicators of its efficiency. While high magnetization requires transition metals that are relatively inexpensive and abundant, rare-earth elements (REs) are typically used to ensure a high magnetic anisotropy energy, which is linked to the coercivity of the sample. The main drawback of magnets with rare earths concerns their high cost, the scarcity of raw materials (rare earths), and the global distribution of these ores. These resources, located in relatively restrained areas around the globe, especially in China (with approximately 96% of rare-earth resources

in 2011), tend to become critical raw materials for the economies of the European Union and US [1].

The RT_{12}-based compounds with tetragonal $ThMn_{12}$ structure type (1:12 structure, space group *I4/mmm*) (R = rare earth, T = transition metal) continue to be considered as attractive candidates for permanent magnet (PM) applications [2,3]. Significant magnetization and Curie temperature are found in the compounds with T = Fe, while the tetragonal structure allows for strong uniaxial anisotropy, which is obtained in particular for R = Sm. These materials have the potential to be used as permanent magnets due to their intrinsic magnetic properties and high transition metal to rare-earth element ratio (>75%). Nevertheless, the 1:12 structure needs to be stabilized by the Fe substitution with elements like V, Ti, and Mo because the RFe_{12} compounds are not thermodynamically stable [4]. Light elements such as hydrogen, nitrogen, or carbon can be added to unit cells to improve their magnetic properties. In particular, these additions may increase the Curie temperature and uniaxial anisotropy, making them suitable for permanent magnet and high-density magnetic recording applications [5–8].

Early investigations of Ohashi et al. [9] show a saturation magnetization of 65 emu/g and a Curie temperature of 483 K for the $SmFe_{10}Mo_2$ compound, which are both lower than the values from other $Sm(Fe,M)_{12}$ compounds with M = Cr, V, and Si. Müller [10] found for $Sm_8Fe_{80}Mo_{12}$ alloy a Curie temperature of 475 K, saturation magnetization of 0.97 T estimated from the magnetization curves, and an anisotropy field H_a of about 6–8 MA/m. The coercivity of $ThMn_{12}$-type magnets was studied by Schultz and Wecker [11]. According to their studies, the $Sm_{12}Fe_{78}Mo_{10}$ multiphase sample has the highest coercivity value of 3.8 kOe, indicating that significant coercivity may be produced in such samples, although still not sufficient for practical use [11]. Later studies of Kou et al. [12] on $SmFe_{10}Mo_2$ alloy reported values of 430 K for Curie temperature and 18.4 μ_B/f.u. for saturation magnetization at 4.2 K. An anisotropy field Ba = 4.8 T (at 300 K) of $SmFe_{10}Mo_2$ compound has been determined directly from a peak in the curve d^2M/dB^2 vs. B [13], which is further enhanced by the reduction of the Mo content. Isnard and Guillot [14] investigated the magnetic properties of $SmFe_{10}Mo_2$ and $SmFe_{10}Mo_2H$ compounds, finding uniaxial behavior at room temperature in both compounds, with the c-axis as the easy axis direction. Based on the magnetization vs. magnetic field dependency at 4.2 K, magnetization values of 13.58 μ_B/f.u. for $SmFe_{10}Mo_2$ and 14.65 μ_B/f.u. for $SmFe_{10}Mo_2H$ have been determined. Anisotropy constants K_1 and K_2 have been estimated for polycrystalline samples at 300 K, showing an increase in K_1 from 2.2 to 3.0 MJ/m^3 by H addition. The K_2 anisotropy constants at 300 K are one order of magnitude lower than K_1, with values of 0.18 MJ/m^3 for $SmFe_{10}Mo_2$ and 0.2 MJ/m^3 for $SmFe_{10}Mo_2H$. This behavior could be explained by an enhancement of the Sm sublattice anisotropy by H addition. Additionally, in $SmFe_{10}Mo_2H$ compound at 4.2 K, an even 10% higher anisotropy constant K_1 was obtained (3.4 MJ/m^3), whereas hydrogenation raised the K_2 constant at 0.26 MJ/m^3.

Khazzan et al. [15] explored the nanostructured $Sm(Fe,Mo)_{12}$ phases, finding that the $ThMn_{12}$ tetragonal phase is possible only if the annealing temperature in the preparation procedure exceeds 900 °C. They identified a novel hexagonal $Sm(Fe,Mo)_{12}$ phase with a maximum coercive field H_c of 5 kOe, a semi-hard magnetic material with potential applications in magnetic recording.

Recently, Xu et al. [16] investigated the effects of Co on the magnetic properties of $SmFe_{10.5-x}Co_x$ $Mo_{1.5}$, including the Curie temperature, saturation magnetization M_s, anisotropy field Ha, and energy product $(BH)_{max}$. They found that Co substitution leads to an increase in the Curie temperature and saturation magnetization but decreases the anisotropy field and coercivity.

In this work, we present our results of the theoretical investigation on the intrinsic properties of the $SmFe_{12-x}Mo_x$ (x = 1, 2) and $SmFe_{10}Mo_2H$ compounds. The calculated magnetic moments, magneto-crystalline anisotropy energy (MAE), and exchange-coupling parameters are analyzed. We applied the coherent potential approximation (CPA) within the spin-polarized, fully relativistic Korringa–Kohn–Rostoker (SPR-KKR) band structure

approach to deal with the substitutional disorder. In order to account for the significant correlation effects caused by the *4f* electronic states of Sm, the present method includes Hubbard-U correction to the local spin density approximation (LSDA+U). Based on the calculated exchange-coupling parameters, a rough estimation of the Curie temperature based on the mean field approach is obtained. Our goal in examining these systems is to obtain a further understanding of the substitution effect of Mo for Fe and the impact of H addition on the intrinsic magnetic properties of the current alloys. This research contributes to efforts to develop an appropriate method for describing the magnetic properties of $Sm(Fe,M)_{12}$ alloys and their hydrides, which boils down to an accurate description of the Sm *4f* states and Fe sublattices, which is required for predicting suitable candidates for permanent magnet applications.

2. Methods

The Munich SPRKKR band structure program package [17] has been used to perform electronic band structure calculations within the Density Functional Theory [18]. Multiple scattering theory is applied in KKR–Green's function formalism, providing the basis for the theoretical calculations [18]. The fully relativistic approach was used, which means that all relativistic effects were considered, including spin-orbit coupling. The angular momentum expansion of the basis functions was taken up to l = 3 for Sm and l = 2 for Fe and Mo. The exchange and correlation effects have been accounted for by means of the local spin density approximation using the parametrization of Vosko et al. [19], as the previous theoretical investigations [6,20] show that this is more suitable for the description of magnetic properties of 1:12 phases. The k-space integration was performed using the special points method [21]. A mesh of 15 × 15 × 15 points in the Brillouin zone was used for self-consistent calculations. The substitutional disorder in the system has been treated within the Coherent Potential Approximation (CPA) theory [22]. Atomic spheres approximation (ASA) has been used for self-consistent band structure calculations, assuming overlapping atomic spheres, inside which the electronic charge is spherically symmetric [23].

Moreover, electron correlations that are not fully included in the LSDA have been systematically accounted for beyond the LSDA. The LSDA+U method [18] was used to account for the on-site Coulomb interactions caused by Sm's localized *4f* electrons. Czyżyk and Sawatsky's atomic limit expression [24] was used to handle double-counting. The Hubbard U and Hund exchange J parameters were parametrized with values of 7.0 eV and 0.9 eV, respectively, which were sufficient for splitting the *4f* orbital bands into lower and higher Hubbard bands. Similar U and J values were utilized in recent LSDA+U theoretical computations for Sm in 1:12 alloys [20,25].

In addition, the magnetic torque method has been used to analyze the magnetic anisotropy. The magnetic torque directed in the magnetization direction $\vec{M}$ [26,27] and acting on the $\vec{m_i}$ magnetic moment of the atomic site i was considered. The component of the magnetic torque with respect to axis $\hat{u}$ is defined by $T_{\hat{u}}(\theta, \varphi) = -\partial E$, where θ and φ are the polar angles. The magnetic torque and the energy difference between the in-plane and out-of-plane magnetization orientations can be related by a particular geometry. To determine the magnetic torque for uniaxial anisotropy, the angles are set to $\theta = \pi/4$ and φ = 0, and the calculated magnetic torque is $T_{\hat{u}}(\pi/4, 0) = E_{[100]} - E_{[001]}$ [27]. A denser mesh of 25 × 25 × 25 k-points in the Brillouin zone was used for the magnetic anisotropy calculations.

For a ferromagnetic crystal with uniaxial symmetry, the magneto-crystalline anisotropy energy up to the second order has the expression:

$$E_a = K_1 sin^2\theta + K_2 sin^4\theta, \quad (1)$$

where θ is the polar angle. In our calculations, the energy difference $E_{[100]} - E_{[001]}$ is computed [27] by the torque method, which corresponds to an anisotropy constant $K_u \approx K_1 + K_2$.

A complementary method for exploring the magnetic behavior of solids is to consider microscopic models to describe the magnetic interaction. A commonly used technique relies on the formula that describes the classical Heisenberg Hamiltonian:

$$H_{\mathrm{ex}} = -\sum_{\mathrm{ij}} J_{\mathrm{ij}} \hat{e}_i \cdot \hat{e}_j \quad (2)$$

where the summation is performed on all lattice sites i and j, and $\hat{e}_i/\hat{e}_j$ are the unit vectors of magnetic moments on sites i and j, respectively. The expression developed by Liechtenstein [28] from the magnetic force theorem has been used to calculate the J_{ij} exchange-coupling parameters for the Fe and Sm magnetic moments as a function of distance. The Curie temperatures were estimated using the mean field approach [28,29] by the following expression [30]:

$$T_c^{rough-MFA} = \frac{2}{3k_B}\sum_i J_{0i} \quad (3)$$

The J_{0i} exchange-coupling parameters in this expression are obtained through applying the summation of J_{ij} on all coordination shells up to 15 Å surrounding lattice site i. The summing over all lattice sites yields the Curie temperature according to Equation (3).

3. Results and Discussions

3.1. Crystal Structures

The $SmFe_{12-x}Mo_x$ (x = 1, 2) and $SmFe_{10}Mo_2H$ compounds crystallize in the $ThMn_{12}$ structure (space group *I4/mmm*) with Fe atoms on three inequivalent crystal sites (*8i*, *8j*, and *8f*) and the Sm atoms on *2a* sites (Figure 1). The role of Mo atoms is to stabilize this type of structure, as the $SmFe_{12}$ compound is not stable [4]. The Mo atoms preferentially occupy the *8i* sites [4,14]. On the other hand, by hydrogenation of the $SmFe_{10}Mo_2$ compound, the H atoms preferentially occupy the octahedral *2b* sites [14] (Figure 1). The number of atoms in the unit cell corresponds to the multiplicity of the occupied positions (Sm-*2a* and Fe-*8i*, *8j*, and *8f*) resulting in 26 atoms/cell and 13 atoms/f.u. The atom number in the cell increases to 28 (14 atoms/f.u.) by adding H to the 2b site.

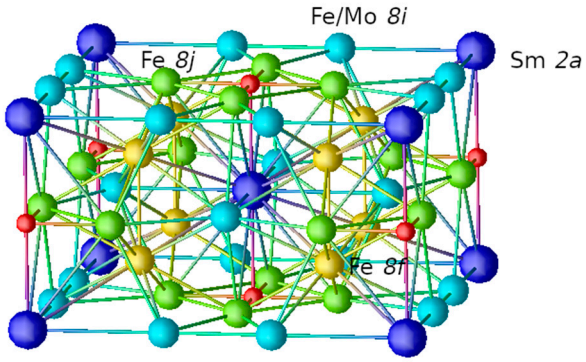


Figure 1. The $ThMn_{12}$ type of structure of $SmFe_{10}Mo_2H$ compound. The Sm atoms on *2a* sites (dark-blue spheres), Fe/Mo atoms on *8i* sites (light-blue spheres), and Fe atoms on *8j* and *8f* sites (green and yellow spheres, respectively). By H addition in $SmFe_{10}Mo_2$ compound, the inserted H atoms (small red spheres) occupy the *2b* sites, with *2a* and *8j* sites as nearest neighbors.

Raising the Mo content and adding H both cause the lattice constants increase [14,31,32]. The theoretical calculations use the experimental lattice constants [14] summarized in Table 1. The internal coordinates x_{8i} = 0.358 and x_{8j} = 0.278 for $SmFe_{10}Mo_2$ have been used to create the structure of the investigated alloys [15]. Table 1 also shows the muffin-tin radius for each type of atom as ASA calculations are performed.

Table 1. Lattice constants of the $SmFe_{12-x}Mo_x$ (x = 1, 2) and $SmFe_{10}Mo_2H$ compounds. The muffin-tin radii for each type of atom are displayed.

	a_{lat} (Å)	c_{lat} (Å)	r_{MT}^{2a} (Å)	r_{MT}^{8i} (Å)	r_{MT}^{8j} (Å)	r_{MT}^{8f} (Å)	r_{MT}^{2b} (Å)
$SmFe_{11}Mo$ [31]	8.548	4.772	1.615	1.216	1.230	1.196	-
$SmFe_{10}Mo_2$ [14]	8.587	4.798	1.605	1.219	1.234	1.199	-
$SmFe_{10}Mo_2H$ [14]	8.605	4.816	1.580	1.221	1.219	1.204	0.691

3.2. Density of States

Band structure calculations using the SPR-KKR band structure method have been performed for $SmFe_{12-x}Mo_x$ (x = 1, 2) and $SmFe_{10}Mo_2H$ alloys. The density of states (DOS) calculated by the LSDA and LSDA+U approaches for $SmFe_{10}Mo_2$ and $SmFe_{10}Mo_2H$ alloys, respectively, are presented in Figure 2.

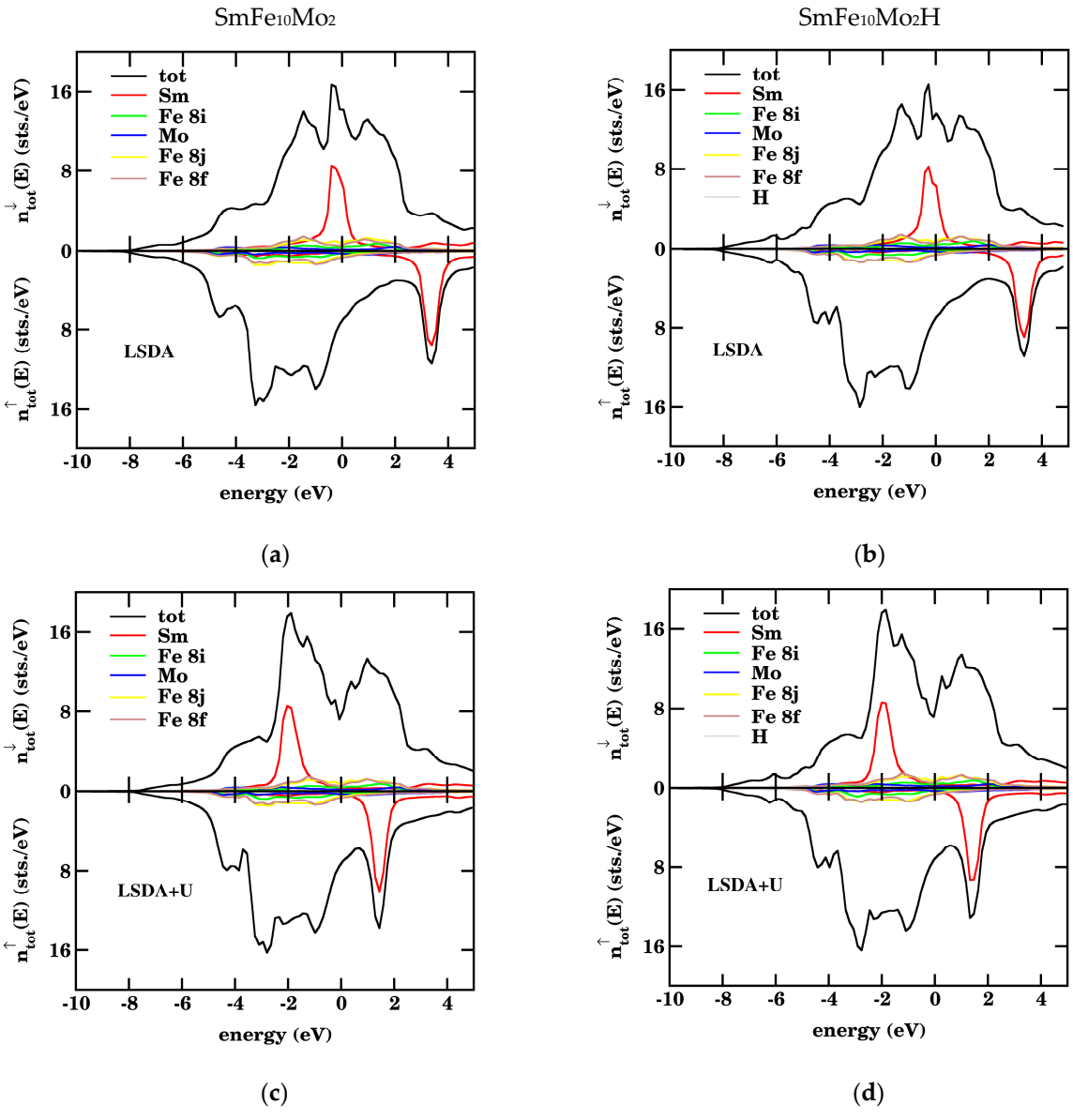


Figure 2. The density of states of $SmFe_{10}Mo_2$ by the LSDA (**a**) and LSDA+U (**c**) approach, respectively. Similar density of states plots for the $SmFe_{10}Mo_2H$ alloys by LSDA (**b**) and LSDA+U (**d**) approaches are shown. The Fermi level is the origin of the energy scale.

The DOS plots for $SmFe_{10}Mo_2$ and $SmFe_{10}Mo_2H$ alloys show that the LSDA fails to describe the strongly localized *4f* orbitals of Sm, which are pinned at the Fermi level. The LSDA+U method splits Sm's f-orbitals into lower and upper Hubbard bands. The spin-up Sm-*4f* bands are unoccupied, while only the Sm-*4f* spin-down bands are occupied, indicating that the Sm spin moments align opposite the Fe spin moments. The separation between the spin-down and spin-up *4f*-bands of Sm is given by *U–J* energy value. Antiparallel alignment between Sm and Fe spins is also seen in the LSDA-calculated DOS, due to the unoccupied Sm-*4f* spin-up bands above the Fermi level.

3.3. Magnetic Moments

The calculated magnetic moments for $SmFe_{12-x}Mo_x$ (x = 1, 2) and $SmFe_{10}Mo_2H$ alloys are shown in Table 2. The Sm spin moments obtained by the LSDA approach show absolute values that are close to the ideal spin magnetic moment of the $4f^6$ electronic configuration (6 μ_B). On the other hand, by the LSDA+U approach, the spin moment of Sm antiparallel aligned with the Fe spin moments (as shown by DOS calculations) is lowered in absolute magnitude, with values of −5.17 μ_B (x = 1), −5.11 μ_B (x = 2) for the $SmFe_{12-x}Mo_x$ (x = 1, 2) compounds, and −5.07 μ_B for the $SmFe_{10}Mo_2H$ compound. These values for the Sm spin moment are in agreement with previous LSDA+U calculations for other $Sm(Fe,M)_{12}$ alloys with $ThMn_{12}$ structure type [25,33]. In addition, the present calculations satisfy Hund's third rule for less than half-filled *4f*-shells [34], which states that the Sm orbital moment is antiparallel with the Sm spin moment.

Table 2. Atom type-resolved and total calculated magnetic moments (in Bohr magnetons μ_B) for $SmFe_{11}Mo$, $SmFe_{10}Mo_2$, and $SmFe_{10}Mo_2H$ alloys. Preferential occupation of Mo for *8i* has been considered. The calculated total magnetization M_s (in A/m) and $\mu_0 M_s$ (in T) are shown. The experimentally determined saturation magnetization (in μ_B/f.u.) is also shown.

	$SmFe_{11}Mo$				**$SmFe_{10}Mo_2$**				**$SmFe_{10}Mo_2H$**			
	LSDA		**LSDA+U**		**LSDA**		**LSDA+U**		**LSDA**		**LSDA+U**	
	m_s (μ_B)	**m_l (μ_B)**	**m_s (μ_B)**	**m_l (μ_B)**	**m_s (μ_B)**	**m_l (μ_B)**	**m_s (μ_B)**	**m_l (μ_B)**	**m_s (μ_B)**	**m_l (μ_B)**	**m_s (μ_B)**	**m_l (μ_B)**
Sm	−5.65	2.81	−5.17	4.83	−5.59	2.88	−5.11	4.79	−5.56	2.84	−5.07	4.78
Fe *8i*	2.41	0.07	2.39	0.05	2.33	0.08	2.40	0.07	2.38	0.09	2.44	0.07
Mo *8i*	−0.56	0.01	−0.58	0.00	−0.39	0.01	−0.43	-	−0.37	0.01	−0.41	-
Fe *8j*	2.19	0.08	2.17	0.06	2.05	0.08	2.09	0.06	1.97	0.08	2.02	0.06
Fe *8f*	1.76	0.05	1.79	0.04	1.64	0.06	1.70	0.05	1.78	0.07	1.82	0.05
H	-	-	-	-	-	-	-	-	−0.02	-	−0.02	-
Total (μ_B/f.u.)	16.82	3.57	17.23	5.36	13.08	3.65	13.98	5.37	13.45	3.62	14.35	5.39
M_{tot}^{theor} (μ_B/f.u)	20.40		22.59		16.73		19.35		17.07		19.74	
M_s^{exp} (μ_B/f.u)					13.58 [14] [a] 18.4 [12] [a]				14.65 [14] [a]			
M_s^{theor} (10^6 A/m)	1.08		1.19		0.88		1.02		0.88		1.03	
$\mu_0 M_s^{theor}$ (T)	1.35		1.49		1.10		1.28		1.11		1.29	

[a] Determined at 4.2 K.

The LSDA approach determined Sm orbital moments in the $SmFe_{11}Mo$ and $SmFe_{10}Mo_2$ compounds of 2.81 μ_B and 2.88 μ_B, respectively. The orbital moments of Sm are underestimated by the LSDA computations. The LSDA+U approach significantly increases the Sm orbital moments to 4.83 μ_B (x = 1) and 4.79 μ_B (x = 2), respectively. The orbital moments calculated by LSDA+U show good agreement with the Sm orbital moment as determined by Hund's rule (5 μ_B). The H addition has less impact on the orbital moment

of Sm; the calculated values in $SmFe_{10}Mo_2H$ compound are 2.84 μ_B by LSDA and 4.78 μ_B by LSDA+U. Our investigation found that the total magnetic moments of the Sm atom resulting from the LSDA+U calculations in the $SmFe_{11}Mo$, $SmFe_{10}Mo_2$, and $SmFe_{10}Mo_2H$ compounds were 0.34, 0.32, and 0.29 μ_B, respectively. The LSDA+U values are slightly lower than the theoretical magnetic moment of the Sm^{3+} ion determined from Hund's third rule (0.71 μ_B) [34,35]. However, the LSDA calculations significantly overestimate the predicted Sm^{3+} total moment due to the orbital moment being lower than Hund's rule estimates.

The Fe spin magnetic moments on the three crystallographic sites are in the sequence m_s^{Fe} (*8i*) > m_s^{Fe} (*8j*) > m_s^{Fe} (*8f*), the lowest value of m_s^{Fe} (*8f*) being related to the shortest interatomic distances around the *8f* site, similar to other calculations for $R(Fe,M)_{12}$ alloys (R = Y, Gd, Sm; M = Ti, V) [6,25,33,36]. A similar magnitude sequence is found in $R(Fe,M)_{12}$ alloys by Mössbauer measurements [37–39] (R = Y, Sm; M = Ti, V).

Such a hierarchy of the magnetic moments of the three inequivalent sites has been explained as resulting from the local environment [40]. In particular, the much larger magnetic moment on the Fe located in the *8i* position has been assigned to the existence of a major ligand line, as well as the large Wigner–Seitz volume on that Fe atomic position. The Mo for Fe substitution decreases the magnetic moments on Fe sites by both LSDA and LSDA+U calculation methods, in agreement with the experimental findings for $R(Fe,M)_{12}$ alloys [4,41]. As a consequence, the total spin moment decreases by increasing the Mo content from 16.82 to 13.08 μ_B by LSDA calculations and from 17.23 to 13.98 μ_B by LSDA+U calculations. A comparison of the site-resolved Fe magnetic moments indicates that this behavior is mostly caused by Fe *8j* and Fe *8f* spin moments dropping.

Interatomic distances rise with H addition due to an increase in the lattice constant a_{lat}. The H inserted atoms on *2b* sites have Fe on *8j* sites as nearest neighbors. Consequently, Fe *8j* spin magnetic moments are particularly affected, being decreased by H addition. On the other hand, the Fe *8i* and Fe *8f* spin magnetic moments increase due to the increase of interatomic distances, as seen in Table 1. According to the LSDA calculation, the spin moments of Fe atoms change by H addition from 2.33, 2.05, and 1.64 μ_B to 2.38, 1.97, and 1.78 μ_B for the *8i*, *8j*, and *8f* sites, respectively. A similar change is shown by the LSDA+U calculations by H addition for the *8i*, *8j*, and *8f* sites (from 2.40, 2.09, and 1.70 μ_B to 2.44, 2.02, and 1.82 μ_B, respectively). Therefore, the total magnetic moment of the $SmFe_{10}Mo_2H$ compound is slightly increased by H addition. This is in agreement with the experimental measurements of Isnard et al. [14]. Still, the total magnetic moments obtained in our calculations show higher values compared with the experimental data at 4.2K for $SmFe_{10}Mo_2$ and $SmFe_{10}Mo_2H$ compounds [14]. An improved agreement of our calculated total magnetic moments with the experimental data of Kou et al. [12] (18.4 μ_B/f.u.) is obtained.

The calculated total magnetic moments of $SmFe_{12-x}Mo_x$ (x = 1, 2) and $SmFe_{10}Mo_2H$ compounds were used to determine saturation magnetization M_s^{theor} (A/m) and $\mu_0 M_s^{theor}$ (T). As previously reported, due to the thermodynamic instability of RFe_{12} compounds (R = rare earth or Y), substituting *3d* elements or metalloids for Fe in order to stabilize the resulting alloy has a detrimental impact on magnetization [4]. This effect is seen in our calculations since the calculated total magnetic moment decreases as the concentration of Mo increases, as shown in Table 2. On the other hand, our theoretical calculations show that the minor increase in the total magnetic moment combined with the volume increase caused by H addition results in a modest rise in the saturation magnetization (from 1.10 to 1.11 T by LSDA calculations and from 1.28 to 1.29 T by LSDA+U calculations).

3.4. Magneto-Crystalline Anisotropy

When considering the use of permanent magnets, one of the most crucial quantities is the magneto-crystalline anisotropy energy (MAE). In order to investigate the microscopical origin of MAE, the magnetic anisotropy constants K_u were decomposed into the rare-earth contribution (Sm atoms sitting on the *2a* crystallographic sites), the contributions of Fe/Mo

atoms from the *8i* sites, the Fe atoms on the *8j* and *8f* crystallographic sites, as well as the H atoms from the *2b* sites (Table 3).

Table 3. The calculated site-resolved contribution to MAE (in meV/atom) for investigated alloys.

	$SmFe_{11}Mo$		$SmFe_{10}Mo_2$		$SmFe_{10}Mo_2H$	
	LSDA	**LSDA+U**	**LSDA**	**LSDA+U**	**LSDA**	**LSDA+U**
Sm 2a	18.67	17.94	17.52	16.21	14.48	18.70
Fe/Mo 8i	0.08	0.05	0.08	0.08	0.02	0.08
Fe 8j	0.30	0.64	0.40	0.63	0.42	0.55
Fe 8f	−0.11	−0.15	−0.05	−0.05	−0.05	0.01
H 2b	-	-	-	-	0.01	0.02
K_u (meV/f.u.)	19.76	21.12	19.22	18.85	16.04	21.28
K_u (MJ/m^3)	9.0	9.2	8.7	8.6	7.2	9.5
K_u^{exp} MJ/m^3			2.4 [a] [14]		3.2 [a] [14], 3.7 [b] [14]	

[a] Determined at 300 K; [b] Determined at 4.2 K.

The magnetic behavior of R-M compounds (R—rare-earth and M—transition metal elements) is mainly determined by two contributions, one given by localized *4f* electrons and the other by itinerant electrons of transition metal elements. Sm atoms have an orbital moment in the presence of spin-orbit coupling, as well as an electron distribution that deviates slightly from the spherical shape. The crystal field acts on the nonspherical electron distribution, fixing the direction of the *4f* orbital moment. The spin-orbit coupling of rare earth is strong enough to rigidly couple the rare-earth spin to the aspherical charge distribution of the *4f* shell.

According to the crystal field theory, the magnetic anisotropy energy expression developed to describe these interactions is mainly determined by (i) the first Stevens coefficient α_J and (ii) A_2^0-the second-order crystal field parameter. In particular, the charge distribution of the Sm *4f* orbitals has a prolate shape along the c-axis, giving rise to a positive Stevens coefficient α_J [35,42–44]. Furthermore, the non-spherical local environment of surrounding ions generates a crystal field that acts on the charge distribution, which is described by the second-order crystal field parameter A_2^0.

The second-order crystal field parameter A_2^0 is negative if the charge along the c-axis is positive (attractive for the electrons) and positive otherwise [35].

As can be seen in Table 3, the anisotropy constants of Sm are positive for all investigated compounds. According to the crystal field theory, the positive anisotropy constants of Sm are given by the positive Stevens coefficient α_J, as well as the negative crystal field parameter A_2^0, similar to other Sm $(Fe,Ti)_{12}$ alloys [45,46]. Our calculations show that the Sm weight at the total anisotropy constant K_u is over 85%.

The Fe/Mo site-resolved K_u contributions are much smaller compared with those of Sm. It can be observed that the Fe *8j* atoms have the highest K_u contribution, whereas the Fe *8f* atoms have a negative contribution at the total anisotropy energy for $SmFe_{12-x}Mo_x$ (x = 1, 2) compounds. The general sequence for anisotropy constants in the investigated compounds is $K_u(8j) > K_u(8i) > 0 > K_u(8f)$. A further characteristic is that LSDA+U computations increase the Fe *8j* contributions compared to LSDA. Similar values for the Fe atom contribution at MAE have been obtained by theoretical investigations of other $Sm(Fe,M)_{12}$ alloys (M = V, Co) [25].

The main influence of H is to modify A_2^0, because H is the nearest neighbor of Sm, which induces a lattice expansion and modifies the charge distribution around the rare earth. The change is reflected in both LSDA and LSDA+U calculations, but only the LSDA+U approach can capture the experimental results, which show an increase in K_u due to H addition in the $SmFe_{10}Mo_2H$ compound. On the other hand, both LSDA and

LSDA+U calculations show a decrease in the anisotropy constant K_u with an increase in the Mo content x in the samples as a result of replacement of Fe atoms by non-magnetic Mo atoms.

When comparing theoretical and experimental anisotropy constants, one must consider that the calculated $K_u \approx K_1 + K_2$. According to experimental measurements, the K_1 anisotropy constant prevails, being about one order of magnitude higher than K_2 [14]. Also, one should take temperature into account since, at low temperatures, the rare-earth sublattice contribution predominates, whereas at high temperatures, the transition metal sublattice contribution prevails. However, the theoretical LSDA+U-calculated anisotropy constants show qualitative agreement with the experimental measurements at 300 K, showing an increase by H addition in the $SmFe_{10}Mo_2H$ compound [14]. Low-temperature measurements of anisotropy constants are only available for the $SmFe_{10}Mo_2H$ compound, which are in qualitative agreement with theoretical results.

One has to note that the present approach based on the atomic sphere approximation (ASA) describes the MAE effects, which stem from spin-orbit coupling and hybridization with ligands. The effects of the anisotropic crystal field arising from the non-spherical potential are neglected. Despite this drawback, the overall trends in magneto-crystalline anisotropy behavior sound reasonable. The above results show that the description of the Sm *4f* electronic state by LSDA+U is essential for MAE calculations in $SmFe_{12-x}Mo_x$ alloys and their hydrides.

In conclusion, all investigated compounds show a uniaxial magnetization orientation, in agreement with previous reports [9,12,14,16]. Similar axial magnetic anisotropy was found in other $R(Fe,M)_{12}$ compounds with R = Sm and M = V or Ti [5,39,46].

3.5. Exchange-Coupling Parameters and CURIE Temperatures

The exchange-coupling parameters (J_{ij}) between Fe spins from *8i*, *8j*, and *8f* sites vs. distance (in units of lattice constant *a*) calculated using Lichtenstein's approach [28] based on the magnetic force theorem are shown in Figure 3. For $SmFe_{11}Mo$, $SmFe_{10}Mo_2$, and $SmFe_{10}Mo_2H$ compounds, the exchange interaction parameters between Fe spins are distinctly shown when Fe *8i*, Fe *8j*, or Fe *8f* spins are considered in the origin. Similar to other 1:12 magnetic phases, the exchange interaction between Fe *8i*-Fe *8i* spins has the highest strength, followed by the exchange interaction between Fe *8i*-Fe *8j*; the magnitude of the other exchange interactions between pairs of Fe spins is lower. An analogous magnitude range of the exchange interactions has been obtained for other $RFe_{11}Ti$ (R = Y, Gd) compounds [36]. When the spin–spin distance exceeds the lattice constant *a*, the J_{ij} parameters decrease significantly and finally drop off. By H addition, the exchange-coupling parameters in particular between Fe *8j*-Fe *8f* and Fe *8j*-Fe *8j* spins (with less negative contributions) are enhanced. On the other hand, an increase in Mo content has a negative impact on the Fe *8i*-Fe *8j* and Fe *8j*-Fe *8j* exchange interactions.

The Curie temperatures deduced by mean field approximation (MFA) [28–30] for $SmFe_{11}Mo$, $SmFe_{10}Mo_2$, and $SmFe_{10}Mo_2H$ alloys are 684 K, 581 K, and 622 K, respectively. It is known that the MFA computations overestimate the Curie temperatures by roughly 20%, and this shortcoming must be taken into consideration when comparing the results with the experimental data [47]. The $SmFe_{11}Mo$ compound's experimental Curie temperature is 551 K [31], whereas the $SmFe_{10}Mo_2$ compound T_c is between 430 K [12,14] and 483 K [9]. The Curie temperature is mainly determined by the Fe-Fe exchange interactions, which are slightly enhanced by H addition. The experimental Curie temperature determined for $SmFe_{10}Mo_2H$ is 476 K [14]. The theoretical calculations obtained qualitative agreement with experimental results, showing a similar magnitude sequence of the Curie temperatures for the investigated compounds. Interestingly, the T_c increase predicted by the theoretical calculation is about 7%, a magnitude similar to the 10% increase observed experimentally. Such reinforcement of the Curie temperature upon H insertion has also been observed in other $Sm(Fe,M)_{12}$ compounds [32,37] and is general for such a family of $R(Fe,M)_{12}$ compounds [8,37].

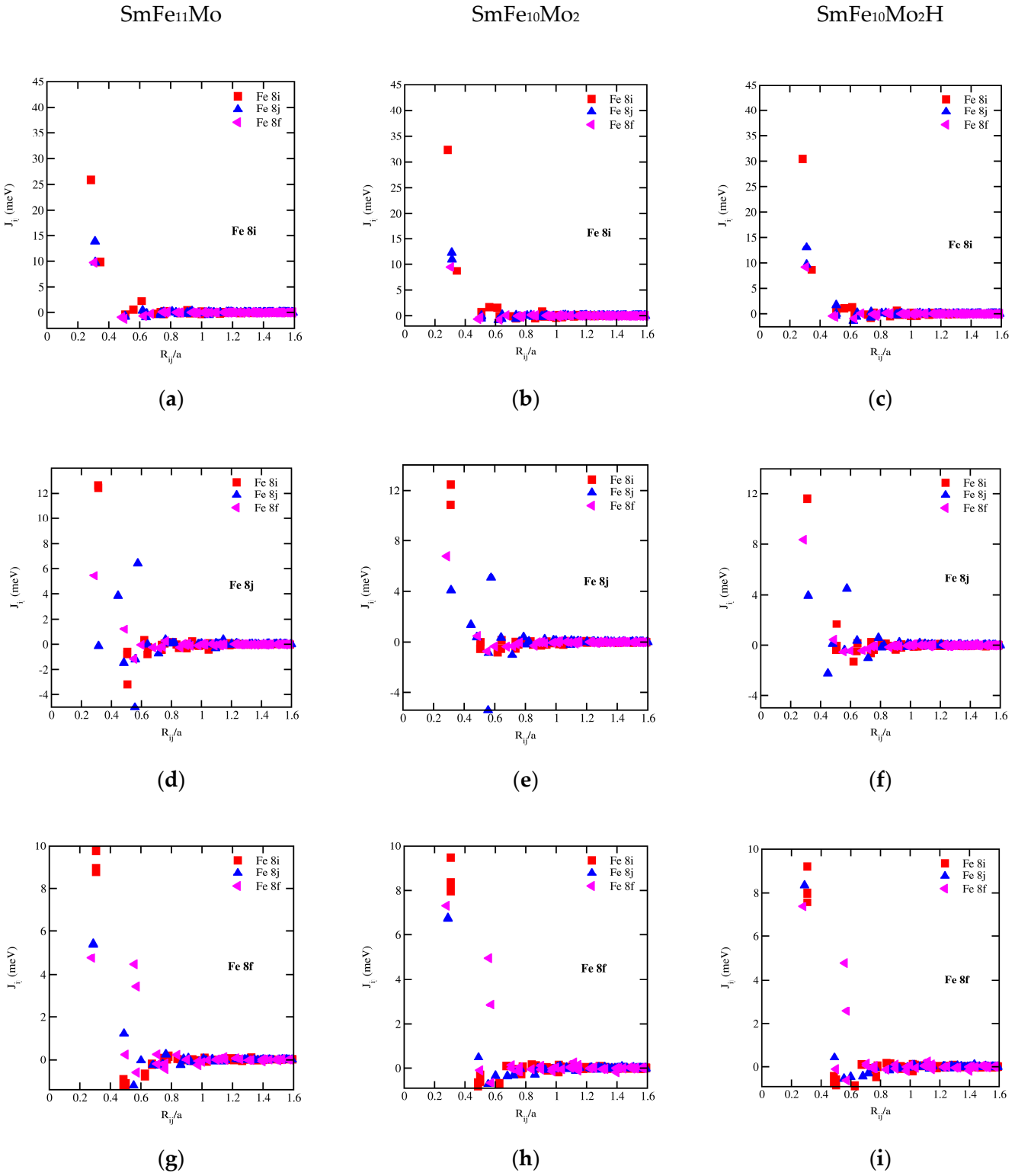


Figure 3. The exchange-coupling parameters *Jij* between Fe spins from *8i*, *8j*, and *8f* sites for $SmFe_{10}Mo_2$ and $SmFe_{10}Mo_2H$ compounds. The exchange interactions are considered within a sphere of *1.6a* radius (a-lattice constant) around each site. Fe *8i* (**a**–**c**), Fe *8j* (**d**–**f**), and Fe *8f* (**g**–**i**) spins are considered in the origin.

4. Conclusions

Fully relativistic Korringa–Kohn–Rostoker (SPR-KKR) band structure method calculations using the LSDA+U approach to account for the correlation effects due to the *4f*

electronic states of Sm have been performed for $SmFe_{12-x}Mo_x$ (x = 1, 2) and $SmFe_{10}Mo_2H$ compounds. The density of state calculations shows unoccupied spin-up Sm-*4f* bands and occupied Sm-*4f* spin-down bands, indicating that the Sm spin moments align opposite the Fe spin moments. The Sm spin moments obtained by the LSDA+U approach show absolute values that are lower than the ideal spin magnetic moment of the $4f^6$ electronic configuration (6 μ_B). The orbital moments calculated by the LSDA+U approach show good agreement with the Sm orbital moment as determined by Hund's rule (5 μ_B). The Fe spin magnetic moments on the three crystallographic sites are in the sequence m_s^{Fe} (*8i*) > m_s^{Fe} (*8j*) > m_s^{Fe} (*8f*) in all investigated compounds, with the lowest value of the m_s^{Fe} (*8f*) being related to the shortest interatomic distances around the *8f* site. The total spin moment decreases by increasing the Mo content, while the H addition is slightly increasing it. The minor increase in the total magnetic moment combined with the volume increase caused by H addition results in a modest rise in the saturation magnetization of $SmFe_{10}Mo_2H$. All investigated compounds show a uniaxial magnetization orientation, in agreement with previous reports, with Sm contributing over 85% at the total anisotropy constant K_u. The Fe and Mo contributions are much lower, with an anisotropy constant sequence of $K_u(8j) > K_u(8i) > 0 > K_u(8f)$ obtained for $SmFe_{12-x}Mo_x$ (x = 1, 2) compounds. Our calculations show a decrease in the anisotropy constant K_u with an increase in the Mo content x in the samples, as well as a slight increase in K_u by H addition in the $SmFe_{10}Mo_2H$ compound. These trends well reproduce the behavior reported earlier on the basis of experimental studies. The Curie temperatures deduced by mean field approximation (MFA) are in qualitative agreement with experimental results, showing a similar magnitude sequence of the Curie temperatures for the investigated compounds.

Author Contributions: Conceptualization, D.B. and O.I.; methodology, D.B.; software, D.B.; validation, D.B., O.I. and V.P.; formal analysis, D.B. and O.I.; investigation, D.B.; resources, D.B.; data curation, E.B.; writing—original draft preparation, D.B.; writing—review and editing, D.B., O.I. and V.P.; visualization, D.B. and E.B.; supervision, D.B. All authors have read and agreed to the published version of the manuscript.

Funding: Funding from the Ministry of Research, Innovation and Digitization by CCCDI-UEFISCDI grant PN-III-P2-2.1-PED-2019-3484 is acknowledged.

Data Availability Statement: Additional data are available by request.

Conflicts of Interest: The authors declare no conflicts of interest. The funders had no role in the design of the study; in the collection, analyses, or interpretation of data; in the writing of the manuscript; or in the decision to publish the results.

References

1. Report on Critical Raw Materials for the EU 2014. Available online: https://rmis.jrc.ec.europa.eu/uploads/crm-report-on-critical-raw-materials_en.pdf (accessed on 3 June 2024).
2. de Mooij, D.B.; Buschow, K.H.J. Some novel ternary $ThMn_{12}$-type compounds. *J. Less-Common Met.* **1988**, *136*, 207–215. [CrossRef]
3. Coey, J.M.D. Perspective and prospects for rare earth permanent magnets. *Engineering* **2020**, *6*, 119–131. [CrossRef]
4. Buschow, K.H.J. Permanent magnet materials based on tetragonal rare earth compounds of the type $RFe1_{2-x}M_x$. *J. Magn. Magn. Mater.* **1991**, *100*, 79–89. [CrossRef]
5. Harashima, Y.; Terakura, K.; Kino, H.; Ishibashi, S.; Miyake, T. Nitrogen as the best interstitial dopant among, C, N, O, and F for strong permanent magnet: First-principles study. *Phys. Rev. B* **2015**, *92*, 184426. [CrossRef]
6. Ke, L.; Johnson, D.D. Intrinsic magnetic properties in $R(Fe_{1-x}Co_x)_{11}$ Ti Z (R = Y and Ce; Z = H, C, and N). *Phys. Rev. B* **2016**, *94*, 024423. [CrossRef]
7. Tomey, E.; Isnard, O.; Fagan, A.; Desmoulins, C.; Miraglia, S.; Soubeyroux, J.L.; Fruchart, D. Modulation of spin reorientation transitions in the series $R(Fe,M)_{12}Xy$ (R = Y, Nd, Ho; M = Mo, Ti; X = N, H). *J. Alloys Compd.* **1993**, *191*, 233–238. [CrossRef]
8. Isnard, O.; Pop, V. Effect of hydrogen as interstitial element on the magnetic properties of some iron rich intermetallic compounds. *J. Alloys Compd.* **2011**, *509*, S549–S554. [CrossRef]
9. Ohashi, K.; Tawara, Y.; Osugi, R.; Shimao, M. Magnetic properties of Fe-rich rare earth intermetallic compounds with a $ThMn_{12}$ Structure. *J. Appl. Phys.* **1998**, *64*, 5714. [CrossRef]
10. Müller, A. Magnetic material R,Fe,Mo,(Co) with $ThMn_{12}$ structure. *J. Appl. Phys.* **1998**, *64*, 249–251. [CrossRef]
11. Schultz, L.; Wecker, J. Coercivity in $ThMn_{12}$ type magnets. *J. Appl. Phys.* **1988**, *64*, 5711. [CrossRef]

12. Kou, X.C.; Sinnecker, E.H.C.P.; Grössinger, R.; Wiesinger, G.; Zhao, T.; Liu, J.P.; de Boer, F.R. Magnetocrystalline anisotropy of $SmFe_{12-x}Mo_x$ compounds with x = 0.5, 1.0, 1.5, 2.0 or 3.0. *J. Magn. Magn. Mater.* **1995**, *140–144*, 1025–1026. [CrossRef]
13. Kou, X.C.; Grössinger, R.; Wiesinger, G.; Liu, J.P.; de Boer, F.R.; Kleinschroth, I.; Krönmüller, H. Intrinsic magnetic properties of R compounds (R = Y, Pr, Nd, Sm, Gd, Tb, Dy, Ho, Er, or Tm). *Phys. Rev. B* **1995**, *51*, 8254. [CrossRef]
14. Isnard, O.; Guillot, M. Investigation of the magnetic properties of $SmFe_{10}Mo_2$ and $SmFe_{10}Mo_2H$ in high magnetic field. *J. Appl. Phys.* **1999**, *85*, 4681–4683. [CrossRef]
15. Khazzan, S.; Bessais, L.; Van Tendeloo, G.; Mliki, N. Correlation between the nanocrystalline $Sm(Fe,Mo)_{12}$ and it's out of equilibrium phase $Sm(Fe,Mo)_{10}$. *J. Magn. Magn. Mater.* **2014**, *363*, 125–132. [CrossRef]
16. Xu, Y.; Hadjipanayis, G.C. Investigation of rare earth lean Sm-(Fe,Co)-Mo alloys for permanent magnets. *J. Magn. Magn. Mater.* **2024**, *589*, 171484. [CrossRef]
17. Ebert, H. The Munich SPR-KKR Package, Versions 7.7 and 8.6. Available online: http://ebert.cup.uni-muenchen.de/SPRKKR (accessed on 4 June 2024).
18. Ebert, H.; Ködderitzsch, D.; Minar, J. Calculating condensed matter properties using the KKR-Green's function method—Recent developments and applications. *Rep. Prog. Phys.* **2011**, *74*, 096501. [CrossRef]
19. Vosko, S.H.; Wilk, L.; Nusair, M. Accurate spin-dependent electron liquid correlation energies for local spin density calculations: A critical analysis. *Can. J. Phys.* **1980**, *58*, 1200–1211. [CrossRef]
20. Herper, H.C.; Skokov, K.P.; Ener, S.; Thunström, P.; Diop, L.V.B.; Gutfleisch, O.; Eriksson, O. Magnetic properties of NdFe11Ti and YFe11Ti, from experiment and theory. *Acta Mater.* **2023**, *242*, 118473. [CrossRef]
21. Monkhorst, H.; Pack, J. Special points for Brillouin-zone integrations. *Phys. Rev. B* **1976**, *13*, 5188. [CrossRef]
22. Faulkner, J.S.; Stocks, G.M. Calculating properties with the coherent-potential approximation. *Phys. Rev. B* **1980**, *21*, 3222. [CrossRef]
23. Andersen, O.K.; Skriver, H.L.; Nohl, H.; Johansson, B. Electronic structure of transition metal compounds; ground-state properties of the 3d-monoxides in the atomic sphere approximation. *Pure Appl. Chem.* **1979**, *52*, 93. [CrossRef]
24. Czyżyk, M.T.; Sawatsky, G.A. Local-density functional and on-site correlations: The electronic structure of La_2CuO_4 and $LaCuO_3$. *Phys. Rev. B* **1994**, *49*, 14211. [CrossRef] [PubMed]
25. Odkhuu, D.; Ochirkhuyag, T.; Hong, S.C. Enhancing Energy Product and Thermal Stability of by Interstitial Doping. *Phys. Rev. Appl.* **2020**, *13*, 054076. [CrossRef]
26. Staunton, J.B.; Szunyogh, L.; Buruzs, A.; Gyorffy, B.L.; Ostanin, S.; Udvardi, L. Temperature dependence of magnetic anisotropy: An ab initio approach. *Phys. Rev. B* **2006**, *74*, 144411. [CrossRef]
27. Mankovsky, S.; Polesya, S.; Minar, J.; Hoffmann, F.; Back, D.H.; Ebert, H. Spin-orbit coupling effect in (Ga,Mn) As films: Anisotropic exchange interactions and magnetocrystalline anisotropy. *Phys. Rev. B* **2011**, *84*, 201201. [CrossRef]
28. Liechtenstein, A.I.; Katsnelson, M.I.; Antropov, V.P.; Gubanov, V.A. Local spin density functional approach to the theory of exchange interactions in ferromagnetic metals and alloys. *J. Magn. Magn. Mater.* **1987**, *67*, 65–74. [CrossRef]
29. Anderson, P.W. Theory of magnetic exchange interactions: Exchange in insulators and semiconductors. *Solid State Phys.* **1963**, *14*, 99. [CrossRef]
30. Nieves, P.; Arapan, S.; Maudes-Raedo, J.; Marticorena-Sánchez, R.; Del Brío, N.L.; Kovacs, A.; Echevarria-Bonet, C.; Salazar, D.; Weischenberg, J.; Zhang, H.; et al. Database of novel magnetic materials for high-performance permanent magnet development. *Comput. Mat. Sci.* **2019**, *168*, 188–202. [CrossRef]
31. Bessais, L. Structure and magnetic properties of intermetallic rare-earth-transition-metal compounds: A review. *Materials* **2022**, *15*, 201. [CrossRef] [PubMed]
32. Tomey, E.; Bacmann, M.; Fruchart, D.; Soubeyroux, J.L.; Gignoux, D. Influence of hydrogen on the structural and magnetic properties of the $RFe_{10.5}Mo_{1.5}$ compounds (R = rare earth). *J. Alloys Compd.* **1995**, *231*, 195–200. [CrossRef]
33. Benea, D.; Pop, V.; Minár, J. The effects of V doping on the intrinsic properties of $SmFe_{10}Co_2$ alloys: A theoretical investigation. *Comput. Mat. Sci.* **2024**, *241*, 113029. [CrossRef]
34. Skomski, R.; Coey, J.M.D. *Permanent Magnetism*; Taylor & Francis Group: Bristol, UK, 1999.
35. Miyake, T.; Akai, H. Quantum theory of rare-earth magnets. *J. Phys. Soc. Jpn.* **2018**, *87*, 041009. [CrossRef]
36. Benea, D.; Hirian, R.; Gutoiu, S.; Isnard, O.; Pop, V. Intrinsic magnetic properties of the $RFe_{11}Ti$ (R = Y and Gd) alloys by Co, Zr and C doping. *Solid State Commun.* **2022**, *355*, 114922. [CrossRef]
37. Piquer, C.; Grandjean, F.; Long, G.J.; Isnard, O. A magnetic and Mössbauer spectral study of $SmFe_{11}Ti$, $LuFe_{11}Ti$, and their respective hydrides. *J. Alloys Comp.* **2005**, *383*, 6–14. [CrossRef]
38. Tereshina, I.S.; Nikitin, S.A.; Ivanova, T.I.; Skokov, K.P. Rare-earth and transition metal sublattice contributions to magnetization and magnetic anisotropy of $R(TM,Ti)_{12}$ single crystals. *J. Alloys Compd.* **1998**, *275–277*, 625–628. [CrossRef]
39. Schönhöbel, A.M.; Madugundo, R.; Vekilova, O.Y.; Eriksson, O.; Herper, H.C.; Barandiaran, J.M.; Hadjipanayis, G.C. Intrinsic magnetic properties of $SmFe_{12-x}V_x$ alloys with reduced V-concentration. *J. Alloys Compd.* **2019**, *786*, 969. [CrossRef]
40. Isnard, O.; Fruchart, D. A review on magnetism in Fe based intermetallics, relation between local environment and local magnetic moments. *J. Alloys Comp.* **1994**, *205*, 1–15. [CrossRef]
41. Rodriguez-Crespo, B.; Garcia-Franco, A.; Rosero-Romo, J.J.; Echevarria-Bonet, C.; Porro, J.M.; Saiz, P.G.; Salazar, D. Magnetic Properties of Tetragonal $SmFe_{12-x}Mo_x$ Alloys in Bulk and Melt-Spun Ribbons. *Phys. Status Solidi A* **2022**, *219*, 2100725. [CrossRef]

42. Stevens, K.W.H. Matrix Elements and Operator Equivalents Connected with the Magnetic Properties of Rare Earth Ions. *Proc. Phys. Soc.* **1952**, *65*, 209. [CrossRef]
43. Skomski, R. *Simple Models of Magnetism*; Oxford University Press: Oxford, UK, 2008.
44. Buschow, K.H.J.; de Boer, F.R. *Physics of Magnetism and Magnetic Materials*; Kluwer Academic Publishers: New York, NY, USA, 2004; ISBN 0-306-47421-2.
45. Diop, L.V.B.; Kuz'min, M.D.; Skourski, Y.; Skokov, K.P.; Radulov, I.A.; Gutfleisch, O. Determination of the crystal field parameters in $SmFe_{11}Ti$. *Phys. Rev. B* **2020**, *102*, 064423. [CrossRef]
46. Tereshina, I.S.; Pankratov, N.Y.; Tereshina, E.A.; Verbetski, V.N.; Salamova, A.A.; Mydlarz, T.; Suski, W. Magnetocrystalline anisotropy of hydrogenated and nitrogenated rare-earth intermetallic compound $SmFe_{11}Ti$. *Phys. Met. Metall.* **2005**, *99*, S46.
47. Sato, K.; Bergqvist, L.; Kudrnovsky, J.; Dederichs, P.H.; Eriksson, O.; Turek, I.; Sanyal, B.; Bouzerar, J.; Katayama-Yoshida, H.; Dinh, V.A.; et al. First-principles theory of dilute magnetic semiconductors. *Rev. Mod. Phys.* **2010**, *82*, 1633. [CrossRef]

Disclaimer/Publisher's Note: The statements, opinions and data contained in all publications are solely those of the individual author(s) and contributor(s) and not of MDPI and/or the editor(s). MDPI and/or the editor(s) disclaim responsibility for any injury to people or property resulting from any ideas, methods, instructions or products referred to in the content.